usually increase this positive miss distance. The unbiased proportional navigation missile experiencing sustain thrust cutoff shortly before intercept may thus develop a large positive angle of attack during terminal encounter. For large crossing angles this may rotate the missile longitudinal axis to the extent that the effectiveness of the warhead is significantly reduced.

References

[1]Cornford, B.A. and Bain, M.A., "The Kinematics of Proportional Navigation Courses for a Missile with a Time Lag," Royal Aircraft Establishment, England, Tech. Note GW85, Oct. 1950.

[2]Paarman, L.O., Farone, J.M., and Smoots, G.W., "Guidance Law Handback for Classical Proportional Navigation," IIT Research Institute, Chicago, Ill, Rept. GACIAC HB-78-01, June 1978.

[3]Pastrick, H.L., Seltzer, S.M., and Warren, M.E., "Guidance Laws for Short-Range Tactical Missiles," *Journal of Guidance and Control,* March-April 1981, pp. 98-108.

[4]Arbenz, K., "Proportional Navigation of Nonstationary Targets," *IEEE Transactions on Aerospace and Electronic Systems,* July 1970, pp. 455-457.

[5]Nesline, F.W. and Zarchan, P., "A New Look at Classical vs Modern Homing Missile Guidance," *Journal of Guidance and Control,* Jan.-Feb. 1981, pp. 78-85.

[6]Smith, W.M., "Preliminary Trajectory Shaping Policy for SM2 Block 11 ER/HAW," General Dynamics, Pomona, Calif., TM 6-331-119.30.1, Jan. 1979.

[7]Chadwick, W.R., "A Theoretical Analysis of Collision Course Navigation with Command Guidance," Weapons Research Establishment, South Australia, Tech. Note SAD 141, Dec. 1964.

Guidance Performance Analysis with In-Flight Radome Error Calibration

William R. Yueh*
Northrop Electronics Division
Hawthorne, California
and
Ching-Fang Lin†
Boeing Company, Seattle, Washington

Introduction

MISSILE homing performance can be seriously degraded by boresight radome errors whose slopes generally show large variations. Thus, to increase homing performance and target intercept capability, in-flight radome error calibration is essential to overcome the restrictions imposed by radome errors.[1-5] This Note presents a self-learning network scheme with an adaptive real-time estimation using a Kalman filter bank design for the switching environment for high-altitude, high-speed threat.

Adaptive Radome Estimator Design

An adaptive Kalman filtering bank in the switching environment is used to realize the changing processes in a radome slope. The rate of switching is assumed to be considerably slower than that of the boresight error (observation) sampling rate. That is, by assuming the rate of positive-negative radome slope switching to be smaller than the data sampling rate, the estimation scheme can be reduced to the design of a bank of Kalman filters, each matched to a certain radome slope configuration. Actually, following the adaptive filter formulation in Refs. 6-8, the random switching of the unreliable plant, i.e., the radome slope is modeled by a semi-Markov process.

A semi-Markov process is a probabilistic system that makes its state transitions according to the transition probability matrix of a conventional Markov process. However, the amount of time spent in each state before the next transition to a different state is a random variable. It is this property of a random switching time that distinguishes the more general semi-Markov process from a Markov process. The multiple states mentioned above are actually chosen to typify the radome slope in the positive, zero, or negative slope regions. Thus, by proper choice of the state and modeling of the transition processes, we hope to realize the variations of the radome slope as a randomly switching, semi-Markov process.

The general adaptive filter, as shown in Fig. 1, essentially consists of a bank of three Kalman filters, each matched to a possible plant configuration U_i $(i=1,2,3)$. The filter outputs are weighted by a time-varying a posteriori probability to obtain the radome error slope estimate. The bank of three Kalman filters has the deterministic inputs $U_1=U_+=0.02$ deg/deg, $U_2=U_0=0.0$ deg/deg, and $U_3=U_-=-0.02$ deg/deg to characterize the three plant configurations in the positive, zero, and negative slope regions, respectively. That is, the filter estimates from each filter in the bank are further weighted by calculating the a posteriori hypothesis probabilities. It is the probability of a given hypothesis that the radome slope is around certain U_i value, being true conditioned upon the past measurements. Since during actual flight the unknown plant configuration (due to polarization effect) might randomly switch at random times, we have to model the random switching of the radome slope parameters as a semi-Markov process. The a posteriori hypothesis testing involves the three conditional probabilities

$$P_{1,k+1}=P_+(U_{k+1}=U_+\,|Z_{k+1})$$
$$P_{2,k+1}=P_0(U_{k+1}=U_0\,|Z_{k+1})$$
$$P_{3,k+1}=P_-(U_{k+1}=U_-\,|Z_{k+1}) \qquad (1)$$

where Z_{k+1} denotes the collective events of all the past measurement history up to time t_{k+1}, i.e.,

$$Z_{k+1}=\{z_1,z_2,\ldots z_k,z_{k+1}\}=\{Z_k,z_{k+1}\} \qquad (2)$$

Equation (1) actually states that for a new boresight datum z_{k+1} that just comes in, we want to test a global hypothesis to see whether the datum indicates that the plant configuration, or the radome slope, is near the positive, zero, or negative slope region. It is a global instead of local hypothesis because it depends on the time history of the data, as shown in Eq. (2). Thus, the a posteriori conditional probabilities should be calculated recursively to reflect all the past data dependence. The detailed formulations are given in Refs. 6 and 7 and are shown below for $i=1,2,3$, as

$$P_{i,k+1}=P(z_{k+1}\,|U_{k+1}=U_i,Z_k)\times \text{normalizing factor}$$
$$\times\sum_{j=1}^{3}[P_{j,k}\times\mathcal{K}_{ij}(t_{k+1}-t_k)] \qquad (3)$$

in terms of the recursive time index k. The normalizing factor is the inverse of the sum of the three a posteriori conditional probabilities. The transition matrix $\mathcal{K}_{ij}$ from state U_i to U_j is symmetric and is based on the semi-Markov statistics. This

Received Oct. 12, 1984; revision received Feb. 19, 1985. Copyright © 1985 by William R. Yueh and Ching-Fang Lin. Published by the American Institute of Aeronautics and Astronautics, Inc., with permission.

*Senior Research Engineer. Member AIAA.
†Lead Engineer, Flight Controls Technology. Member AIAA.

renders a very simple form for in-flight real-time computation and eliminates the computer storage problem that grows with increasing time in the conventional Markov process approach. The first term on the right-hand side of Eq. (3) furnishes the adaptive learning feature of the system. It actually "tests" the new boresight data z_{k+1} to check the probability of being within each plant configuration, i.e., whether it corresponds more to the positive or negative slope region. This conditional probability can be approximated by a Gaussian density for those cases in which the probability of a transition occurring between any two adjacent sampling times is very small. As pointed out in Ref. 6, the actual density is not Gaussian, but is in fact a weighted sum of Gaussian densities. However, it was determined experimentally from computer simulation that even when the plant randomly switched as often as the duration of several system response times, the Gaussian approximation was quite good. The mean and variance of the Gaussian density are recursively determined by the bank of Kalman filter estimates and the associated filter covariance.

Now we come to the discussion of the linear state dynamic equation in Kalman filter modeling, based on the seeker boresight data measurement. Define the look angle as

$$\beta = \sigma - \psi \tag{4}$$

where σ is the true line-of-sight (LOS) angle and ψ the body pitch angle. The measured LOS angle can be denoted by σ_m and is given by

$$\sigma_m = \sigma + \sigma_r(\beta) + \text{noise} \tag{5}$$

where σ_r is the radome aberration error with explicit look-angle dependence. Thus the time derivative of the measured LOS to the first-order linearization approximation can be approximately written as

$$\dot{\sigma}_m = \dot{\sigma} + \frac{\partial \sigma_r}{\partial \beta}\dot{\beta} = \dot{\sigma}(1+r) - r\dot{\psi} \tag{6}$$

where the radome local slope is chosen as

$$r = \frac{\partial \sigma_r}{\partial \beta} \tag{7}$$

This is the state to be estimated. $\dot{\sigma}$ is the true LOS rate and $\dot{\psi}$ the pitch rate. Assuming a type I radio-frequency tracker we can derive

$$\dot{\epsilon} + K_\epsilon \epsilon = \dot{\sigma} \tag{8}$$

The boresight error ϵ is noisy and the derivative can be performed only through a higher-order differential filtering scheme. K_ϵ is the seeker loop gain. Thus the measurement

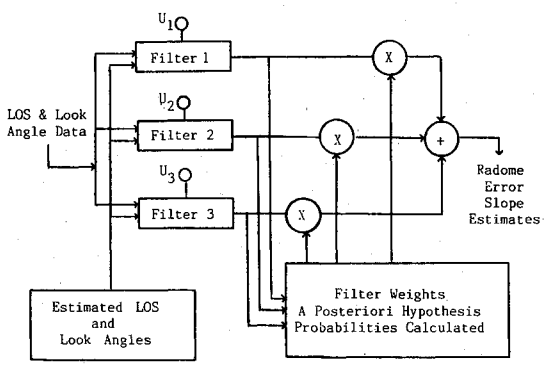

Fig. 1 Adaptive radome error slope estimator (one-state, three-bank Kalman filter).

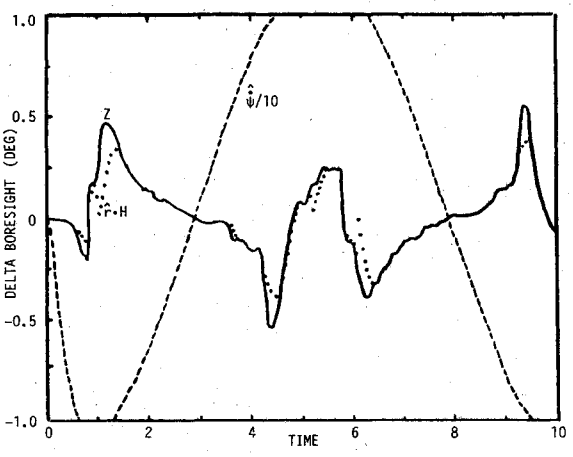

Fig. 2a Comparison of estimated and actual radome errors after matched guidance filtering for sawtooth model.

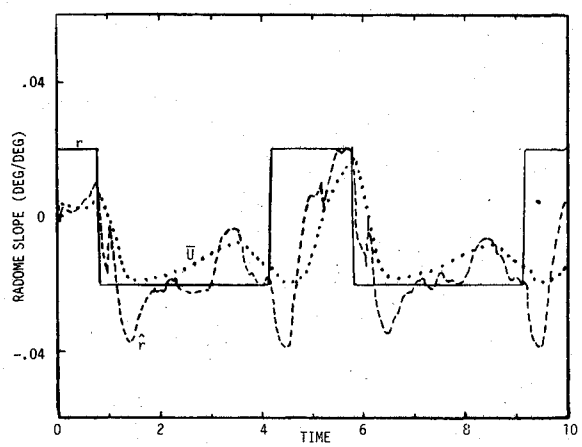

Fig. 2b Estimated and weighted radome error slopes.

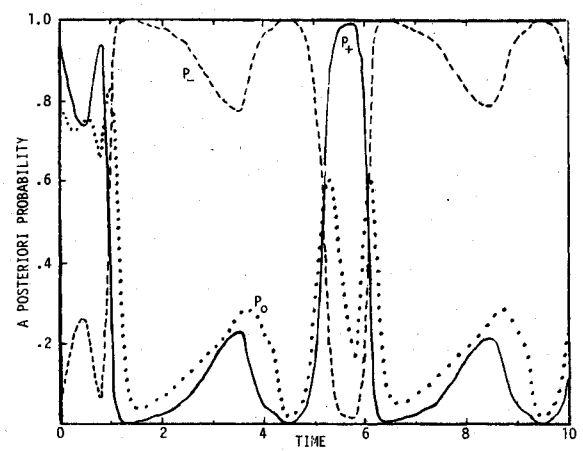

Fig. 2c A posteriori probability for adaptive radome error estimation.

equation can be formalized as

$$Z = r \cdot H + \nu \tag{9}$$

where Z is the smoothed LOS rate from the guidance filtering (of at least second order) output. The measurement partial H is defined as

$$H = -\hat{\dot{\psi}} \tag{10}$$

where $\hat{\dot{\psi}}$ is the smoothed value of $\dot{\psi}$ passing through the same guidance filter. In Eq. (9) the measurement noise ν is the zero

mean white noise Gaussian process with the spectral density equal to the LOS measurement noise spectral density N, i.e., the boresight angular data noise sigma value. For small look angles ($|\beta|<10$ deg), the sequential correlations of the radome error slope can be modeled simply as a random walk process (the correlations are not consistent enough to be modeled),

$$\frac{dr}{dt}=W+\frac{U_i}{\Delta T}, \qquad i=1,2,3 \tag{11}$$

where $\Delta T=t_{k+1}-t_k$ and W is a Gaussian white noise process with plant noise variance defined as, using the Dirac delta function,

$$E[W(t)\cdot W(\tau)]=Q(t)\cdot\delta(t-\tau) \tag{12}$$

where $Q(t)$ is given by the associated standard deviation from table look-up, if available, and may be time varying. In Eq. (11),

$$\frac{dr}{dt}=\frac{d}{dt}\left(\frac{\partial\sigma_r}{\partial\beta}\right) \tag{13}$$

is of higher-order dependence on $\dot{\psi}$ but is neglected in the linear filter approach. The first-order pitch rate dependent term is already included in Eq. (6). For actual flight the auto correlation function for the radome error slope tends to stay constant, rather than exponentially correlated such as that modeled by the Markov process. This is because the typical radome error dependence on look angle is sinusoidal. Thus, the radome error slope can best be modeled as random walk

$$x_{k+1}=x_k+\omega_k \tag{14}$$

The weighted plant input

$$\bar{U}_k=\sum_{i=1}^{3} U_i\cdot P_{i,k} \tag{15}$$

actually represents a very smoothed version of the radome slope estimate and is used in a feedback version [i.e., $\bar{U}$ in Eq. (15) is used in Eq. (16)] to generate a "prediction term" so that Eq. (11) is modified to become

$$\frac{dr}{dt}=\frac{Z-\bar{U}\cdot H}{\beta}+W+\frac{U_i}{\Delta T} \tag{16}$$

The "prediction term" accompanied by the system noise variance is derived based on $\beta=\theta-\psi$ at zero LOS, hence $dr/dt=$ measurement residual$/\beta$, where the measurement residual is equal to $Z-\bar{U}\cdot H$. This additional term has demonstrated improvements in the estimation procedure. The plant noise variance Q is generally determined on-line with radome mapping table look-up. However, for simplicity we assume that Q is identical for the three-plant configurations and can be calculated in the first cut as the table look-up value with respect to the zero mean radome slope. Thus, with the same boresight measurement noise variance R for the three filters, we can easily show that the three Kalman gains are identical if we start with the same initial filter variances. Using the a posteriori probability as the weighting function to weight the estimator outputs and assuming that the weighting coefficients change very little from sample to sample, i.e., $P_{i,k+1}\simeq P_{i,k}$ (this assumption is not well justified if the slope is rapidly changing from sample to sample), we can obtain[7]

$$\hat{r}_{k+1}=\Phi\cdot\hat{r}_k+\bar{U}_k+K_{k+1}\cdot[\hat{\sigma}_{k+1}+\hat{\dot{\psi}}\cdot\Phi\cdot r_k+\hat{\dot{\psi}}\cdot\bar{U}_k] \tag{17}$$

where Φ indicates the operation of radome mapping process and becomes unity in case of no available satisfactory mapping data, i.e., without the prediction term introduced in Eq. (16). Now we essentially reduce the bank of three filters to a single filter with weighted plant input $\bar{U}$ given by Eq. (15).

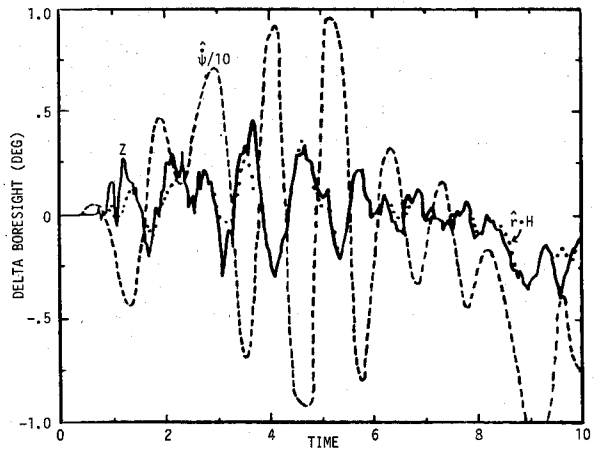

Fig. 3 Comparison of estimated and actual radome errors for realistic data.

Closed-Loop Analysis for Adaptive Radome Estimator

The adaptive estimator results in terminal flight based on an open-loop guidance simulation are plotted in Fig. 2 for a sawtooth radome error slope model. The sawtooth radome error slope model corresponds to the radome error model as a triangular wave function of β, i.e., the radome error varies with the LOS as seen in Eq. (5). In Fig. 2a, the broken curve $\hat{\dot{\psi}}/10$ represents the sinusoidal body pitch rate dependence introduced in the simulation. The dotted curve $\hat{r}\cdot H$ is the reconstructed radome error and follows very closely the boresight error (actual data) Z shown in the solid curve, despite the large noise level chosen (at 0.5 deg/s 1σ level). It has the tendency of cutting the corners when Z goes through sharp spiking behavior. Figure 2b compares the actual radome slope in solid curve r with the estimated radome slope in broken curve $\hat{r}$. A response lag of approximately 1 s can be identified. The estimated slope also tends to overshoot when the actual slope changes sign abruptly. The reason that the estimates degrade near 3 and 8 s is a nulling of the missile body pitch rate, which characterizes the radome error slope sensitivity and provides excitation for the estimator. The weighted plant input $\bar{U}$, as shown by the dots, follows the general trend of the slope estimate and can be denoted as a further smoothed-out version of the estimated slope. The a posteriori probabilities for each plant are shown in Fig. 2c. In Eq. (3), $P_+ + P_0 + P_- = 1$. In actual flight only the negative and positive slopes need calibration, hence in actual implementation of the in-plane radome error calibration scheme only the positive slope probability P_+ and the negative slope probability P_- are used. Therefore, here we normalize the results so that $P_+ + P_- = 1$. The zero slope probability P_0 is still shown here to indicate the trend. Besides the 1 s response lag, the probabilities yield strong indications of the polarity of the slope. For instance, P_- reaches 98% at about 1.2 s after the slope switches at 0.8 s. It starts to degrade because the sensitivity parameter $\hat{\dot{\psi}}$ is getting smaller and thus reduces the variance or confidence level (which is related to the a posteriori probability) in the changing environment.

To check the adaptive filter performance against realistic data, hybrid simulation runs have been made with all the relevant angular information for the specific plane recorded. A six degree-of-freedom simulation was employed with the head-on engagements chosen at 1 deg heading error. There is a 0.5 deg/s 1σ noise level on the LOS rate. The rate gyro bias of 0.05 deg/s appeared on the LOS rate as $\dot{\sigma}_{\text{bias}}$. The radome error slope was a fast-changing process with the signals switching

several times. The body pitch rate manifests more flailing behavior as can be seen from the broken line $\hat{\dot{\psi}}/10$ in Fig. 3. The reconstructed radome error curve $\hat{r}\cdot H$, as shown by the dots, still follows very closely the boresight error (the solid curve Z). The comparison of the estimated slope and the actual one was very difficult due to the ambiguity in the average and local slope calculations during the hybrid run. By not estimating the cross-plane slope simultaneously, we make the missile roll attitude contribution inseparable.

After imbedding this adaptive estimator into terminal guidance forward simulation program to perform the closed-loop analysis, some encouraging results have been obtained. Depending on the actual radome error and the approaching trajectory, the improvement in the miss distance performance index ranges 20-50%. In Ref. 1, the estimated radome error slope is used in guidance and autopilot commands to provide an optimal pitch rate compensation scheme for a modified proportional navigation system and an optimal controller.[2] Using P_+, the probability of radome error being in the positive and negative regions, to scale the pitch rate compensation for enlarging the radome stability region, has also demonstrated reduced excitation in acceleration commands.

Conclusion

A Kalman filter bank is designed to enhance the dynamic response time for the radome error slope estimate with compensation for the seeker dynamic lag. In calculating the critical weighting coefficients (a posteriori probabilities) a measure-predict-measure technique is used when the semi-Markov statistics of a random starting process are used to make the intermediate predictive step. That is, the resulting estimated radome slope parameter is the statistical average weighted by time-varying, a posteriori hypothesis probability, which is calculated concurrently with the recursive filter scheme by using Bayesian rule. To reduce computation burden, the Kalman filter bank is digitally simulated and designed by tuning the noise processes, including the measurement and plant noise, to allow a one-time calculation of the Kalman filter gain. The simple one-state filter described above can be modified to include a correlation parameter for studying the cross-plane errors. The bank of Kalman filters can be increased to five to enlarge the dynamic range while reducing the system response time simultaneously and to estimate the cross-plane radome error slope simultaneously for three-dimensional engagement. The adaptive radome estimator design is intended to be an "add-on" compensation network that is independent of guidance computer and autopilot design. The objective is to permit relaxation of missile bandwidth requirements by reducing error due to radome at the guidance computer output, thus enhancing missile performance.

References

[1]Yueh, W.R. and Lin, C.F., "Bank-to-Turn Guidance Performance Analysis with In-Flight Radome Error Compensation," AIAA Paper 84-1889, Aug. 1984.

[2]Yueh, W.R. and Lin, C.F., "Optimal Controller for Homing Missile," *Journal of Guidance, Control, and Dynamics,* Vol. 8, May-June 1985, pp. 408-411.

[3]Lin, C.F. and Lee, S.P., "Robust Missile Autopilot Design Using a Generalized Singular Optimal Control Technique," *Journal of Guidance, Control, and Dynamics,* Vol. 8, July-Aug. 1985, pp. 498-507.

[4]Yost, D.J., Weckesser, L.B., and Mallalieu, R.C., "Technology Survey of Radomes for Anti-Air Homing Missiles," APL/JHU FS-80-022, March 1980.

[5]Nesline, F.W. and Zarchan, P., "Radome Induced Miss Distance in Aerodynamically Controlled Homing Missiles," AIAA Paper 84-1845, Aug. 1984.

[6]Moose, R.L. and Wang, P.P., "An Adaptive Estimator with Learning for a Plant Containing Semi-Markov Switching Parameters," *IEEE Transactions on Systems, Man and Cybernetics,* Vol. SMC-3, May 1973, pp. 277-281.

[7]Moose, R.L., "An Adaptive State Estimation Solution to the Maneuvering Target Problem," *IEEE Transactions on Automatic Control,* Vol. AC-20, June 1975, pp. 359-362.

[8]Chang, C.B. and Athans, M., "State Estimation for Discrete Systems with Switching Parameters," *IEEE Transactions on Aerospace and Electronic Systems,* Vol. AES-14, May 1978, pp. 418-424.

Controllability and Observability of General Linear Lumped-Parameter Systems

Mehdi Ahmadian*
Clemson University, Clemson, South Carolina

Introduction

THE dynamic behavior of a general linear discrete system can often be represented by the second-order vector differential equation

$$M\ddot{x}(t)+\tilde{C}\dot{x}(t)+\tilde{K}x(t)=0 \tag{1}$$

where M, $\tilde{C}$, and $\tilde{K}$ are the mass, damping, and stiffness matrices. Here, $\tilde{C}$ and $\tilde{K}$ are general asymmetric matrices that include general types of forces (e.g., elastic, nonconservative, dissipative, and gyroscopic).[1] Assuming M to be nonsingular (i.e., det $M\neq 0$), Eq. (1) can be simplified as

$$\ddot{x}(t)+C\dot{x}(t)+Kx(t)=0 \tag{2}$$

where

$$C=M^{-1}\tilde{C} \tag{3a}$$

$$K=M^{-1}\tilde{K} \tag{3b}$$

The presence of control forces modifies the equation of motion as

$$\ddot{x}+C\dot{x}+Kx=f \tag{4}$$

where

$$f=Bu \tag{5}$$

is the $n_a\times 1$ control vector and B is the influence matrix for the n_a control actuators. Additionally, if n_0 sensors are used for separate or mixed measurements of displacement and velocity, then the n_0 sensor outputs can be represented by

$$y=Px+R\dot{x} \tag{6}$$

where y is the output vector and the matrices P and R represent the displacement and velocity influence coefficients, respectively.

It is well known that, based on a first-order formulation of the system, it is possible to mathematically define the controllability and observability of the system as[2]

Received Sept. 24, 1984; revision received Jan. 17, 1985. Copyright © American Institute of Aeronautics and Astronautics, Inc., 1985. All rights reserved.

*Assistant Professor, Department of Mechanical Engineering. Member AIAA.